Pickering emulsions stabilized with two-dimensional (2D) materials: A comparative study

Danae Gonzalez Ortiz, Celine Pochat-Bohatier, Julien Cambedouzou, Mikhael Bechelany, Philippe Miele

Pickering Emulsions Stabilized with Two-Dimensional (2D) Materials: A Comparative Study

Danae Gonzalez Ortiz[1], Celine Pochat-Bohatier[1], Julien Cambedouzou[1,2], Mikhael Bechelany[1,*] and Philippe Miele[1,3*]

[1]Institut Européen des Membranes, IEM UMR-5635, ENCSM, CNRS, University of Montpellier, Place Eugene Bataillon, 34095, Montpellier, France

[2]ICSM, CEA, CNRS, ENSCM, University of Montpellier, 30207, Marcoule, France;

[3]Institut Universitaire de France, IUF, 1 Rue Descartes, 75231, Paris, cedex 5, France

Keywords: Pickering emulsions, graphene oxide, hexagonal boron nitride, particle wettability

Abstract

In this paper, we study the preparation of Pickering emulsions using two-dimensional (2D) materials: graphene oxide (GO) and hexagonal boron nitride nanosheets (h-BNNS). The type of the obtained emulsions, the droplet size and the rheological behavior were investigated for both GO and h-BNNS based emulsions. The results show that two types of emulsion, direct oil-in-water (O/W) and indirect water-in-oil (W/O) may be produced due to the different hydrophilic properties of the 2D materials. Besides, similar microstructures and droplet size are obtained, as well as analogue rheological behaviors. Thus, depending on the potential application, it is possible to tune the emulsion type, W/O or O/W, by choosing the 2D material possessing the most interesting properties for the sought application.

1 Introduction

Two-dimensional (2D) nanosheets have been receiving great attention in recent years due to their ultrathin structure with infinite planar dimensions and their outstanding properties [1-3]. The advantage of these materials is that they have great potential in a huge range of applications at scientific and technological levels in relation to the possibility to be exfoliated as single- or few-layers. The most known 2D layered material and most widely studied is graphene. It is composed by a one-atom thick planar sheet of sp^2 hybridized carbon atoms. Recently other materials, such as layered transition metal dichalcogenides (LTMDs) (*e.g.*, MoS_2 and WS_2), metal oxides and hexagonal boron nitride (h-BN) have gained a renewed interest in their 2D layered form. Their lamellar structure, with relatively weak bonds between the layers, allows them to be exfoliated into single- and few-layers nanosheets. The importance of the structure and morphology of exfoliated 2D layered materials strongly influences their properties due to their high surface area and quantum confinement effects [4,5] and also their high chemical stability and insulating properties [6].

In this study we focus our attention on graphene and h-BN nanosheets as 2D materials due to their extraordinary properties. Graphene is composed by a single layer of two-dimensional atomic crystals comprising sp^2-bonded carbon structure. Since its discovery in 2004 [1], graphene has been trendy in many areas of science and technology due to its specific physicochemical properties. These include a high specific surface area (2630 m^2/g for single graphene layer) [7], large bandgap (~ 6 eV) [8,9], strong mechanical strength [10], and an excellent thermal and electrical behavior as insulator [11,12]. All these remarkable properties make it suitable in a large range of applications such as high-speed electronic [13], optical devices [14], energy generation and storage [15,16], hybrid materials [17] and chemical sensors [18].

h-BN consists of a structural lattice similar to graphite in that equal numbers of boron (B) and nitrogen (N) atoms alternating substitute carbon (C) atoms. Therefore, boron nitride nanosheets (BNNSs) are basically composed by sheets of sp^2 hybridized layers, organized in honeycomb geometry, with an interlayer distance of *ca*. 0.33 nm. The main difference compared to graphite is that the hexagons of neighboring planes are exactly superposed, while they are shifted in the case of graphite. The bonds within the planes are polar ($N\delta^{-}$-$B^{\delta+}$) and display an important covalent character. The interactions between the planes are weak and of van der Waals type. Recently, the interest of scientist in the BNNSs as 2D nanomaterial has increased because of their advantages compared to graphene. BNNSs show highly polar covalent bonds, while graphene holds nonpolar C-C bonds. The strong B-N bonds give h-BN superior mechanical and thermal properties [19]. BNNSs present great mechanical strengths with a bending elastic modulus of hundreds of GPa [20] and have a thermal conductivity about 2000 W mK^{-1} which is in the same order of magnitude of that of graphene [21]. Moreover, BNNSs present superior chemical and thermal stabilities compared with other 2D materials [22-24]. Different strategies can be used to obtain of h-BN nanostructures, in one hand the nanosheets can be obtained from their precursors [25,26]; on the other hand BNNSs can be obtained by exfoliation from bulk h-BN [27] . The great advantage of h-BN over other 2D materials such as graphene, is its biocompatibility and low cytotoxicity. *In vitro* and *in vivo* assays have confirmed the toxicity of C-based materials to human cells and other living biosystems [28,29]. Alternatively, BN-based materials showed to possess better biocompatibility and lower cytotoxicity [30-32]. In addition, numerous works have been used the advantageous properties of h-BN to prepare functional materials, extending from membranes [33] to composites for different range of applications such as photocatalysis [34], gas separation [35] or tissue engineering [36].

Graphite oxide has a similar layered structure to graphite, but the plane of carbon atoms in graphite oxide is decorated by oxygen-containing groups, which not only expand the interlayer distance but also make the atomic-thick layers hydrophilic. Graphene oxide (GO) can be obtained as a result of exfoliation of graphite oxide in water under moderate ultrasonication [37].

Recent research has established a new application for 2D materials through the formation of emulsions, where they can serve as ultrathin plate-like interfacial stabilizers in two-liquid systems. Huang *et al*. conducted pioneering investigations on the interfacial activity of graphene oxide (GO) at different interfaces, proving the behavior of GO as a colloidal surfactant [38]. Few years later, He *et al*. investigated the different conditions affecting the stability of GO emulsions, such as oil type, sonication, GO concentration and pH values [39]. Imperiali *et al.* investigated a route to create 3D GO frameworks by forming a bi-continuous emulsion stabilized by colloidal GO nanoparticles [40]. Thicket *et al.* studied the stabilization energy associated with GO adsorption for oils with different polarities; they found that GO was better adsorbed in non-polar and aromatic oils [41]. Creighton *et al.* presented a thermodynamic analysis of the behavior of 2D materials at liquid-liquid interfaces [42]. Gonzalez Ortiz *et al.* studied the effect of varying the h-BN concentration, oil/water ratio and sonication time and power on the h-BN Pickering emulsions stability. They showed that emulsions stabilized with h-BNNS were of W/O type [43].

The properties of the solid particles, such as the concentration (or particles amount), shape, size and wettability, play a major role in Pickering emulsion behavior. Among these factors, the particle wettability is a key factor in the type of obtained emulsion and its properties. The particle hydrophilicity determines whether the stabilization of oil-in-water (O/W) or water-in-oil emulsion (W/O) will take place. In the case of 2D nanoparticles, the orientation and flexibility [44] of these particles at the liquid interface also are important. The 2D

nanoparticles are likely oriented with the particles lying flat at the liquid-liquid interface, this conformation allowing the reduction of the interfacial area between the two liquids for a given number of nanoparticles [41]. For this kind of nanostructures, the estimation of the water contact angle differs from systems involving spherical nanoparticles. In this case, different semi-empirical analytical models have been developed to compute surface free energy from measured contact angles such as Fowkes [45] or Owens Wendt Rabel and Kaelbel (OWRK) [46]. Each approach is targeted for measuring surface energies of either low surface energy materials or high surface materials or both [47].

Graphene-based emulsions have been used to fabricate GO-based functional materials with specific structure through emulsion polymerization method [48-50]. GO nanosheets possess an amphoteric nature [51], whereby GO assembles at O/W interfaces, and they will tend to stabilize O/W emulsions.

Depending on the targeted application, this type of emulsions are not suitable, whereas W/O emulsions are needed. Contrarily to graphene, h-BNNSs possess a hydrophobic behavior [52], therefore they will tend to stabilize W/O emulsions. This type of emulsions has great interest due to their potential application for the fabrication of materials with specific structures and performance using inverse emulsions as soft templates. Our group has already report the preparation of porous polymer membranes based on h-BNNS stabilized emulsions [53].

In this work, a study based on the different emulsions of GO and h-BNNS is presented. Depending on the material hydrophilic behavior, two types of emulsions, O/W and W/O, can be prepared using the same biphasic system. The obtained emulsions showed similar droplet size. At higher particle concentration, e.g. 2 wt% of GO and h-BNNS, the emulsion droplets are smaller. The emulsion viscosity is higher at medium values of o/w ratio or dispersed phase volume fraction (Φ_{dp}).

2 Experimental part

2.1 Materials

Hexagonal boron nitride (h-BN) was supplied from Saint Gobain (95 % purity, 325 mesh, 3 µm particle size). Graphite powder (CAS n° 7782-42-5, 99.95 % trace metal basis, < 20 µm), phosphoric acid (H_3PO_4, CAS n° 7664-38-2, 85%, 99.99 % trace metal basis), sulfuric acid (CAS n° 7664-93-9, 99.99 %, H_2SO_4), potassium permanganate (K_2MnO_4, CAS n° 7722-64-7, ACS reagent, ≥ 99.0 %), hydrogen peroxide (H_2O_2, CAS n° 7722-84-1, ≥ 30%), fluorescein sodium salt (CAS n° 518-47-8, Bio-Reagent), methyl red (CAS n° 493-52-7, ACS reagent) and ethyl benzoate (CAS n° 93-89-0, ≥ 99 %, density = 1.045) were supplied from Sigma Aldrich. In all the experiments deionized pure water (18 MΩ) was used.

2.2 Methods

2.2.1 Synthesis of graphene oxide (GO)

Graphene oxide was synthesized from natural graphite powder, following modified Hummer's method. Briefly, 3g of graphite were dispersed in concentrated H_2SO_4:H_3PO_4 (9:1, 400 mL) solution. Then, 18 g of $KMnO_4$ were added gradually to the mixture and it was stirred for 12 h. Later on, the mixture was cooled down to room temperature and 3 mL of H_2O_2 were added. A brown precipitate was observed showing that exfoliation of graphene oxide from graphite was being carried out. After one hour stirring, the GO was separated by centrifugation at 6000 rpm for 10 minutes and the supernatant was decanted away. The resultant precipitates were washed several times with 30% hydrochloric acid and absolute ethanol. Finally, the obtained powder was dried at 50°C for 24 hours to obtain the pure graphene oxide.

2.2.2 Liquid assisted exfoliation of h-BN

h-BN nanosheets were fabricated by liquid phase exfoliation with the assistance of an ultrasounds device (model SONOPLUS HD 3100, 100W, 20 kHz) with a microtip of 3 mm diameter (MS73). Basically, 1.0 g of pristine h-BN micropowder was added into 100 mL of water and then sonicated for 1 hour at 65 % amplitude with pulse off/on 0.5 – 1 s. After the sonication, the whitish suspension was allowed to rest for 30 min, and then the supernatant was collected through centrifuging at 3000 rpm for 15 min. The BNNS product was collected by filtration under vacuum and then dried at 60 °C prior to use.

2.2.3 Emulsion preparation

Pickering emulsions stabilized either with graphene oxide or exfoliated h-BN were prepared following a simple two-step sonication protocol. In a first step, the powder was suspended in water and sonicated for 15 min at 65 % amplitude with pulse off/on 0.5 – 1 s using ultrasounds device. This step ensures the well dispersion of materials in the water. In a second step, ethyl benzoate was added to the suspension with different oil/water ratios (**Table 1**) which were subsequently sonicated with the same equipment for 15 min at 65 % amplitude and pulse off/on 0.5 – 1 s. Depending on the O/W or W/O emulsion, one of the phases was labelled. For O/W emulsions, methyl red dye was added to label the oil phase while for W/O emulsion, fluorescein was used to label the water phase.

Disperse phase volume fraction (Φ_{dp}) = 1 / (1+R) **Equation 1**

where R is the ratio between the oil and the water.

The volume fraction of the disperse phase is influenced by the type of emulsion, in O/W emulsions the disperse phase will be the oil while in W/O water is the disperse phase.

Table 1 GO and h-BNNS emulsions composition

Boron nitride (wt %)	Graphene oxide (wt %)	Ratio o/w
0.5, 1.0, 1.5, 2.0	0.5, 1.0, 1.5, 2.0	1 (R1)
0.5, 1.0, 1.5, 2.0	0.5, 1.0, 1.5, 2.0	0.8 (R0.8)
0.5, 1.0, 1.5, 2.0	0.5, 1.0, 1.5, 2.0	0.6 (R0.6)
0.5, 1.0, 1.5, 2.0	0.5, 1.0, 1.5, 2.0	0.4 (R0.4)
0.5, 1.0, 1.5, 2.0	0.5, 1.0, 1.5, 2.0	0.2 (R0.2)

2.3 Characterization techniques

The X-ray diffraction (XRD) patterns of GO and exfoliated h-BN powders were recorded using a PANalytical Xpert powder XRD system with Cu Kα radiation, a scan speed of 2° min^{-1}, a 2 θ range between 3 and 70°, and a step rate of 0.02° per second. The Fourier transformed infrared (FTIR) spectra were recorded with a NEXUS instrument equipped with an attenuated total reflection (ATR) accessory in the frequency range of 600 − 4000 cm^{-1}. Raman spectra have been obtained from Horiba xplora system with λ= 659 nm.

The kinetic stability of the emulsion was evaluated. For that, the emulsions were stored and observed for 14 days at room temperature. Emulsion Stability Index (*ESI %*) is calculated as the ratio between the volume fraction of emulsion after 14-days equilibration (depicted as the product of the height *H* with the vial section) and the volume fraction of emulsion after 3-h equilibration (H_0), as described by **Equation 2** (boundary between the creamed and serum layers was monitored by naked eyes):

$$ESI = \frac{H}{H_0} 100 \qquad \textbf{Equation 2}$$

The emulsions microstructure and type were characterized by an optical microscope (Olympus BX41, Japan) at 5x magnification and equipped with a digital camera (U-TV1X-2, Olympus, Japan) and by laser microdissection microscopy (LEICA, LMD 6500) with a 10x objective. The pictures were processed using the Image J software to determine the droplet diameter. Mean diameter was calculated over 50 determinations.

3 Results and Discussion

In this section, the structure of the obtained materials, GO and h-BNNS, will be discussed in a first step. Then, the obtained emulsions incorporating these two-dimensional materials will be compared regarding the type of emulsion they are able to form, the droplet size distribution in function of the material concentration, the emulsion stability, and their rheological behavior.

3.1 X-ray diffraction

The oxidation and exfoliation of graphite into graphene oxide was confirmed using XRD technique. The XRD patterns of graphite and graphene oxide are shown in **Figure 1**. The graphite displays a diffraction peak at $2\theta = 26.6$ ° corresponding to the (002) plane, which corresponds to a distance between adjacent layers of 3.34 Å. After the introduction of oxygen functionalities via Hummer's method, the peak shifted to $2\theta = 13.4$ ° corresponding to a *d* spacing of about 6.6 Å (calculated with Bragg's law, **Equation 3**). This increase of interlayer distance is attributed to the intercalation of water molecules between the oxidized graphene layers. The variation of interlayer spacing in GO is the result of variations in the oxidation degree.[54] The width of the more intense peak can also be used to verify the exfoliation degree. The crystallite average size was calculated by the Scherrer equation (**Equation 4**). The calculated results show that the crystallite average size of GO is ~3.7 nm

$$d = \frac{\lambda}{2 \sin \theta}$$ **Equation 3**

where d is the distance between adjacent sheets or layers, λ is the wavelength of the X-ray beam (λ= 0.154nm) and θ is the diffraction angle.

$$D = \frac{0.9 \cdot \lambda}{\beta \cos \theta}$$ **Equation 4**

where D is the crystallite size, λ is the wavelength of the X-ray beam (λ= 0.154nm), β is the FWHM and θ is the diffraction angle.

The disappearance of the Bragg peak corresponding to the in-plane periodicity of carbon atoms (100 peak) in GO might be due to the extensive presence of defects in the graphene structure, caused by the graphene oxidation.

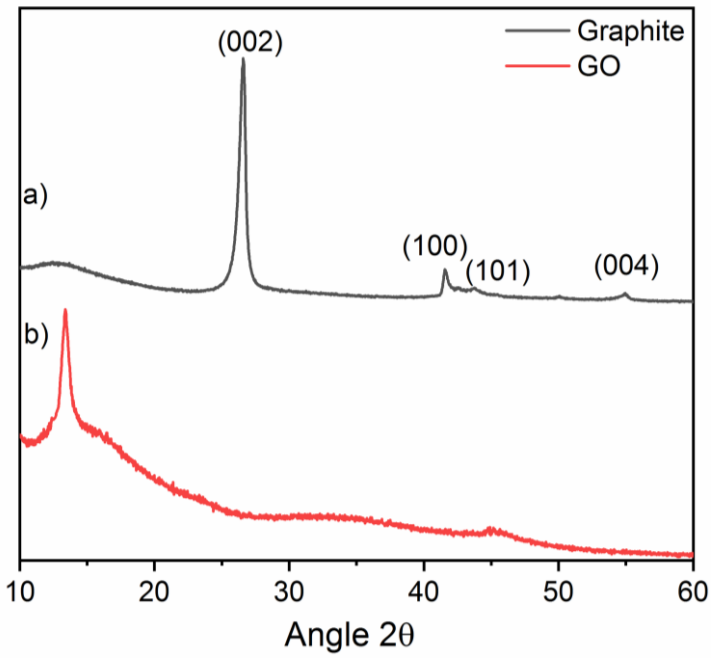

Figure 1 XRD patterns of a) graphite and b) graphene oxide

The XRD patterns of h-BN and h-BNNS are shown in **Figure 2.** The patterns in the **Figure 2a** show the 002, 101, 100 and 004 diffraction peaks of h-BN, which correspond to 2θ angles of 26.71°, 41.6°, 43.8° and 55.1°, respectively. In h-BNNS, the 002 peak is slightly shifted to 2θ = 26.60°. The interlayer distance between layers of h-BN is 3.33 Å, becoming 3.34 Å in h-BNNS. The crystallite average size was calculated by the Scherrer equation (**Equation 4**). The calculated results show that the crystallite average sizes of h-BNNS is ~10.5 nm.

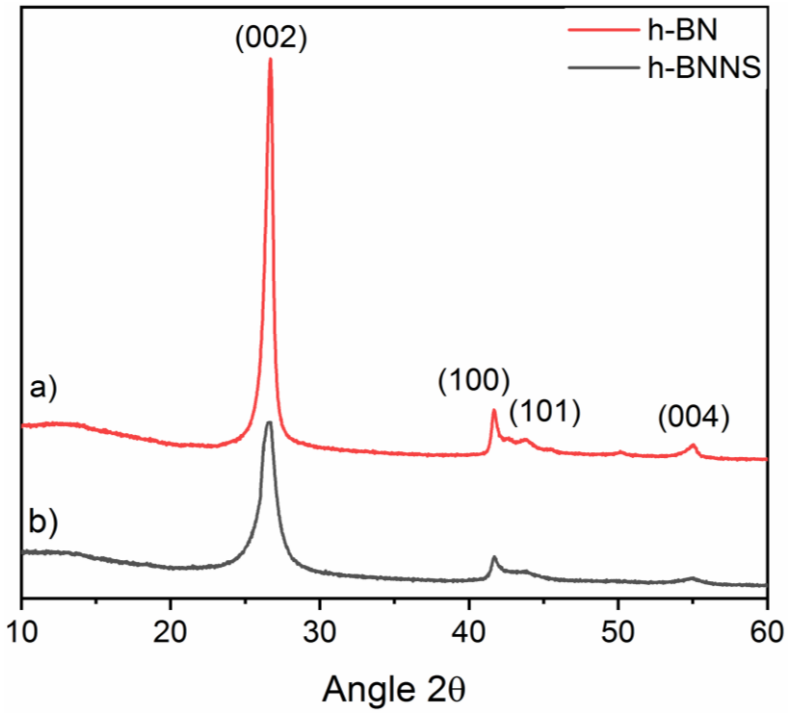

Figure 2 XRD patterns of a) h-boron nitride raw powder and b) h-boron nitride nanosheets

3.2 Fourier-transform infrared spectroscopy

FTIR was employed to identify the functional groups on the GO and h-BNNS surface. The FTIR spectra of graphite and GO are presented in **Figure 3**. In all spectra, the oxidation is confirmed by the presence of several bands attributed to oxygen functionalization. The wide peak at 3396 cm^{-1} is attributed to the -C-OH stretching vibration of hydroxyl group. A second peak located at 1740 cm^{-1} is attributed to the –C=O groups, and the peak at 1617 cm^{-1} to the –

C=C skeletal vibration of non-oxidized graphite. The two absorption peaks at about 1220 cm^{-1} and 1028 cm^{-1} are assigned to the –C-O stretching vibration.[55]

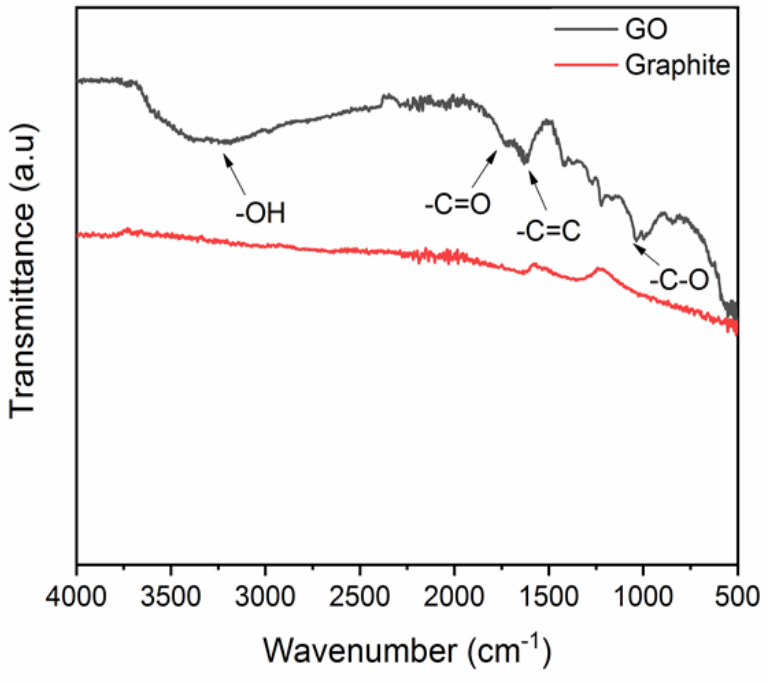

Figure 3 FTIR spectra of graphite and graphene oxide

Figure 4 shows the FTIR spectra of h-BN and h-BNNS. The peak at 812 cm^{-1} can be attributed to B-N stretching (in-plane ring vibration, E_{1u} mode) and the broad absorption at 1380cm^{-1} can be ascribed to the B-N-B bending (out-of-plane vibration, A_{2u} mode). In addition, the h-BNNS spectrum shows another absorption peak at 3200 cm^{-1}, which could be ascribed to hydroxyl group (-OH) vibration. This peak might appear due to the large amount of defects such as vacancy defects, dislocations and exposed edges introduced on the h-BNNS surfaces during sonication.

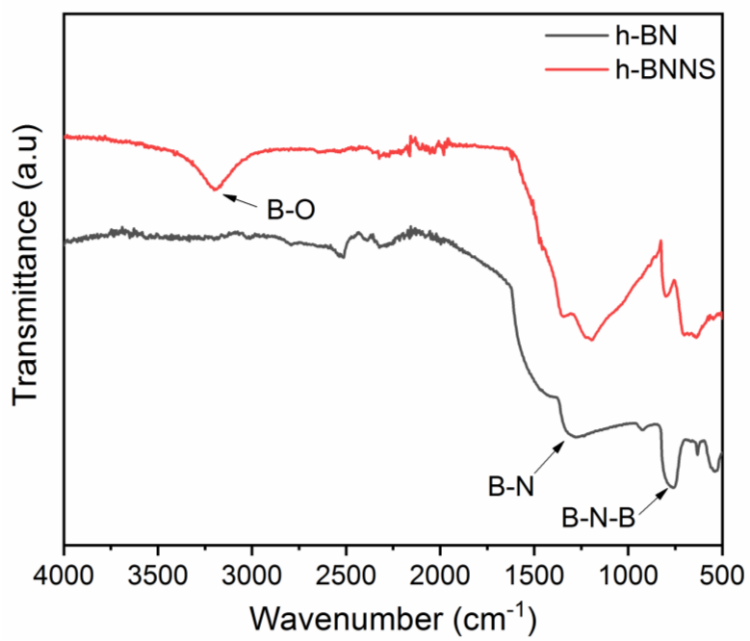

Figure 4 FTIR spectra of h-boron nitride and h-boron nitride nanosheets

3.3 Atomic Force Microscopy

GO obtained after oxidation through Hummer's method and exfoliation was characterized by AFM. A number of about 100 GO nanosheets have been considered for the analysis. **Figure 5** shows the AFM image of GO nanosheets, the results indicate a reduction on the thickness from 20 µm in the case of pristine GO, to 10–30 nm. h-BNNS obtained by exfoliation in water using sonication tip, were characterized as well by AFM. A number of about 100 h-BNNS have been considered for each sample. **Figure 6** shows the AFM image of h-BNNS, the results indicate a reduction on the thickness of pristine h-BN from 3 µm to 2-6 nm. Based on these AFM images and taking into account the width of one GO and h-BN nanosheet (0.33 nm), we could assume that our GO is composed about 30-90 layers; and h-BNNS are generally composed of 3-9 layers.

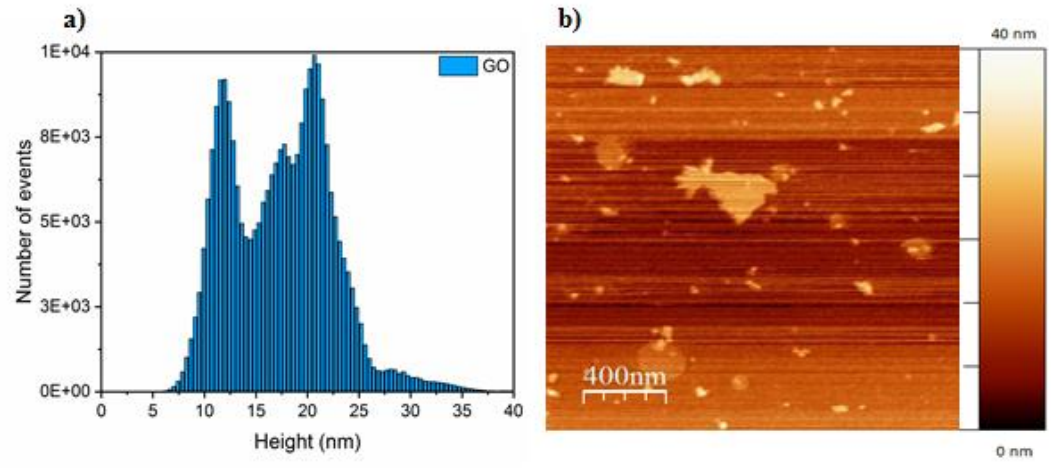

Figure 5 a) AFM image of exfoliated GO and b) height of GO layers

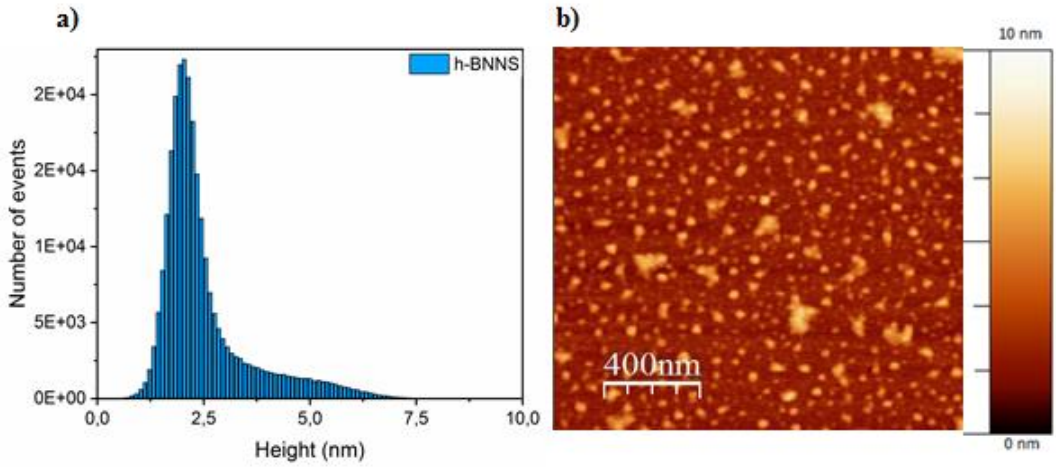

Figure 6 a) AFM image of exfoliated h-BN and) height of h-BNNS layers

3.4 Confocal Laser Scanning Microscopy

The CLSM images of GO and BN with O/W ratio of 1 (R1) are shown in **Figure 7**. The top images are from emulsions stabilized with GO, the oil phase was labelled with methyl red dye. This dye has the ability to be dissolved in ethyl benzoate but it is not soluble in water. It was observed that the droplets display the colored phase, meaning that the disperse phase is composed with the oil and the continuous phase was found to be water. GO nanosheets

therefore turn out to stabilize an oil-in-water (O/W) emulsion. The bottom images are from emulsions stabilized with exfoliated h-BN. In this case, instead of labelling the oil phase, the water phase was labelled with fluorescein dye.

In this case, water was found to be the disperse phase and oil is the continuous phase. Exfoliated h-BN stabilizes water-in-oil (W/O) emulsions. The fact that the 2D materials with such similar morphologies and similar properties behave so differently when stabilizing an emulsion resides in the fact that they display different hydrophilic behaviors.

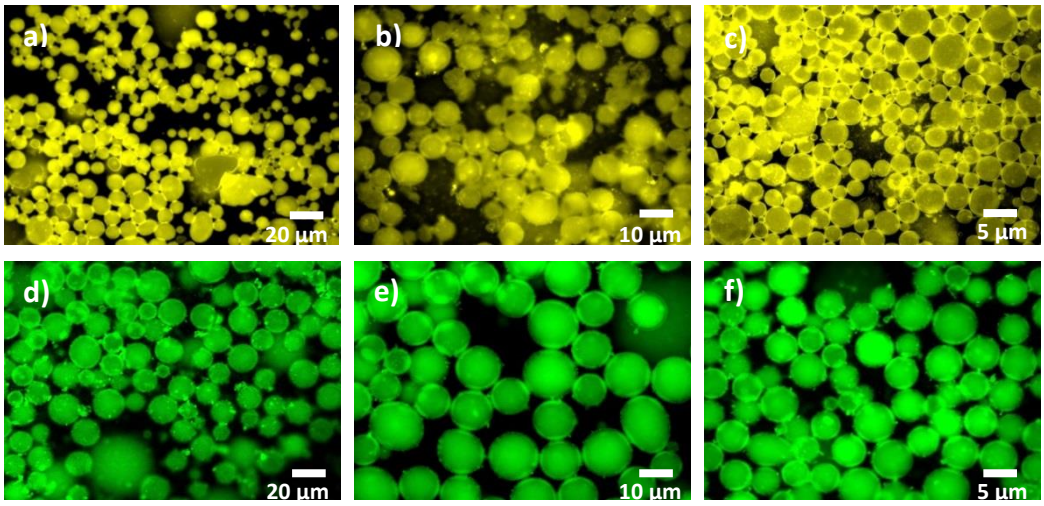

Figure 7 CLSM images of a) 0.5 wt % GO_R1 b) 1.0 wt % GO_R1 c) 2.0 wt % GO_R1 d) 0.5 wt % BN_R1 e) 1.0 wt % BN_R1 and f) 2.0 wt % BN_R1

3.5 Water contact angle measurements

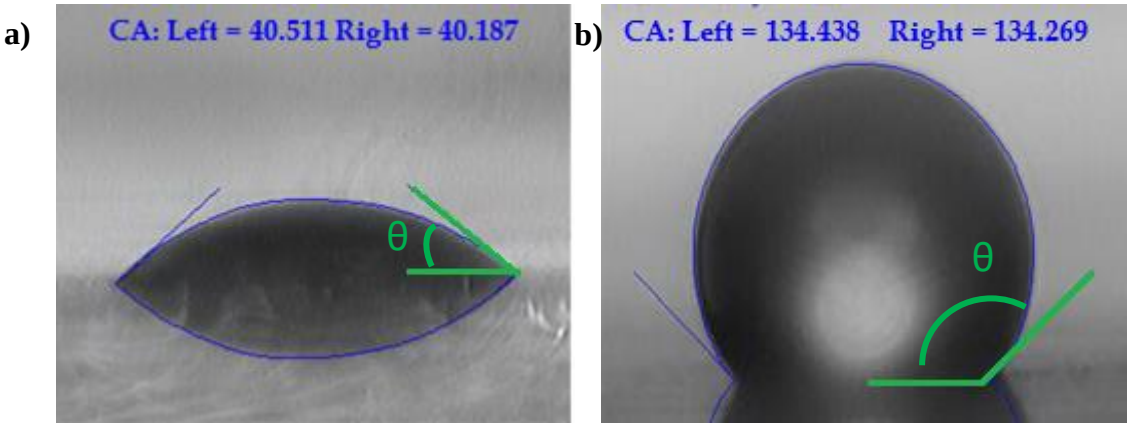

Figure 8 WCA of a) graphene oxide b) h-boron nitride nanosheets powders

The characterization of the wettability was performed using the sessile drop technique by measuring the contact angle between the tangent lines along solid-liquid interface and liquid-vapor interface. The powders were compacted into foam pellets to perform the measurements; for that reason we do not take into account the solid-liquid interfacial tension. In the case were nanoparticles are directly deposited onto a surface, these interactions are playing an important role [47]. **Figure 8**a shows the WCA of GO and **Figure 8**b the WCA of h-BNNS. On one hand, GO displays a hydrophilic behavior with a contact angle around 40.3 ± 0.5 °. The oxygen containing groups such as C-OH and C=O present on the surface will interact with the water molecules while the carbon network (sp^2) will interact with the carbon network of oil (ethyl benzoate) by forming π- π interactions. The nature of the emulsion will be defined depending on the ratio between the C-C groups and C=O groups. In our case, the interactions between oxygen containing groups and water might be stronger, explaining the hydrophilic behavior of GO nanosheets. On the other hand, h-BN shows a hydrophobic behavior with a contact angle of 134.4 ± 0.3 °. In this case, the density distributions of oxygen and hydrogen atoms on the surface of the BN sheet will be very different from those on GO. BN sheets are

more hydrophobic due to the lack of a net dipole normal to the sheet [56]. Also the surface morphology has an influence on the molecule wettability. Ultrasonic exfoliation method was used to obtain the h-BNNS; this method may create defects on the surface making the nanosheets more hydrophobic [57].

3.6 Optical microscopy

The GO and h-BNNS emulsion microstructures and droplets sizes were analyzed by optical microscopy. **Figure 9** shows that the four GO emulsions formulated at different concentrations were successfully used to stabilize O/W Pickering emulsions and they present a relatively homogeneous distribution. The results show that the droplets diameter varies in function of GO concentration from 18 ± 4 µm for the lowest concentration (0.5 wt%) to 6 ± 1 µm for the highest concentration (2 wt%) when the o/w ratio is 1.

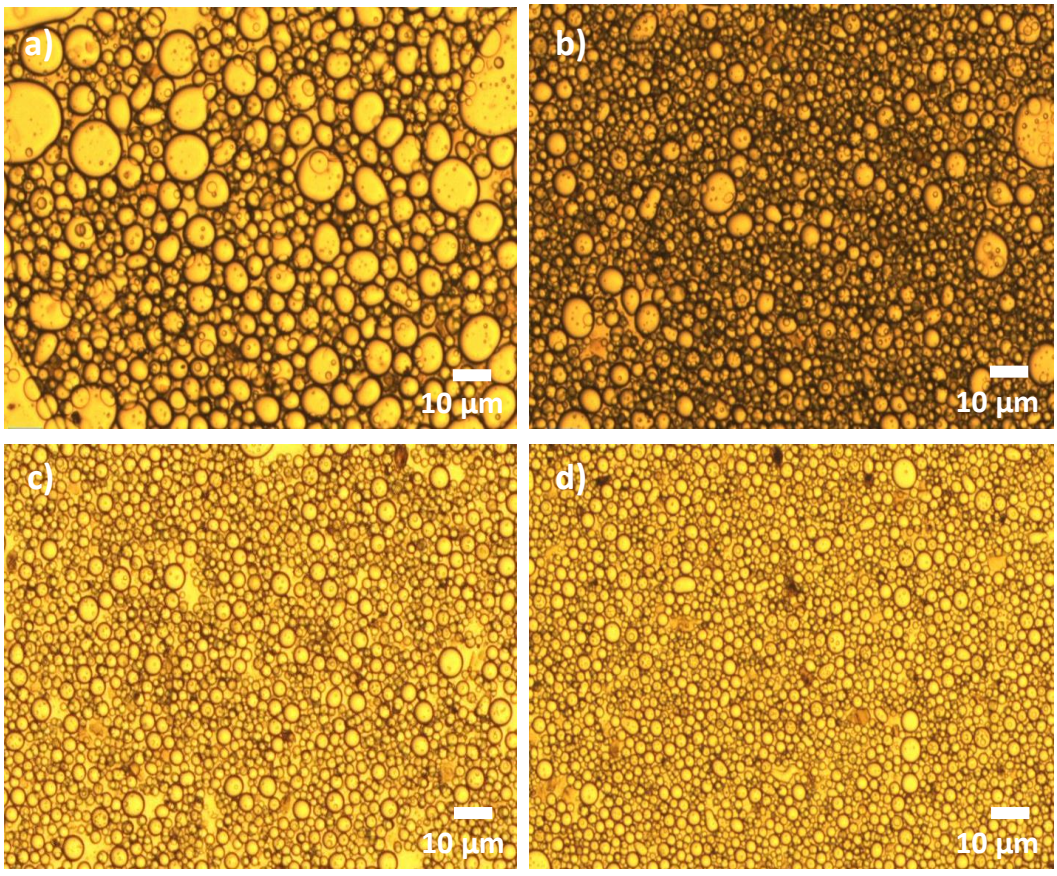

Figure 9 Microscopy images of a) 0.5 wt% GO_R1, b) 1.0 wt% GO_R1 and c) 1.5 wt% GO_R1 and d) 2.0 wt% GO_R1

At low GO concentrations (0.5 wt%), multiple emulsion droplets (w/o/w) were observed. Decreasing the GO concentration may lead to an increase in the number of multi-emulsion droplets and also increase the number of inner w/o emulsion droplets per o/w emulsion droplet. This fact could be related to the different hydrophilic properties of the GO sheets. The degree of oxidation and functionalization can be highly heterogeneous within the GO sheets, thus the amphiphilic properties of each GO sheet also can be different. He *et al.* observed the same effect with emulsion stabilized by GO but it has been reported for low GO mg/ml concentration [39].

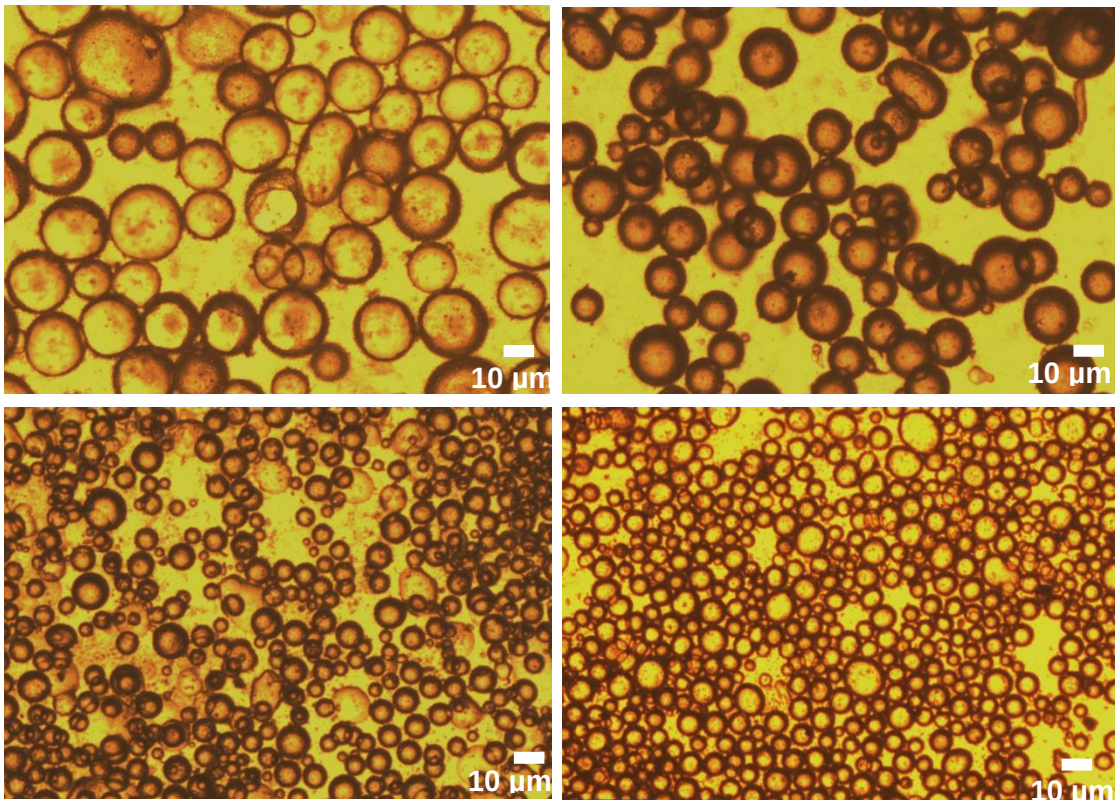

Figure 10 Microscopy images of a) 0.5 wt% BN_R1 b) 1.0 wt% BN_R1 c) 1.5 wt% BN_R1 d) 2.0 wt% BN_R1

Figure 10 shows the microstructure of h-BNNS stabilized emulsions prepared with different concentrations. The images reveal that the h-BNNS successfully stabilized W/O Pickering emulsions and that the droplets present a good homogeneity at high h-BNNS concentrations. At lower concentration, the heterogeneity is greater. These results points out the same behavior than for GO stabilized emulsions, i.e. the droplets diameter decreases as increasing the concentration of stabilizing agent. For emulsions prepared with 0.5 wt% h-BNNS, the emulsion droplets size was found to be 43 ± 5 µm while increasing the concentration up to 2 wt% h-BNNS, the droplets size decreases down to 6.2 ± 0.5 µm.

Both materials are able to stabilize either O/W or W/O emulsions depending on their hydrophilic behavior. It was found that emulsions stabilized with GO are able to form droplets with smaller diameters than those stabilized with h-BNNS (**Figure 11**). This behavior can be explained by the fact that ethyl benzoate is an aromatic solvent, which possesses a carbon sp^2 network. Indeed, GO is composed also by partially broken sp^2-carbon networks and they can interact with the aromatic rings having stronger π-π interactions. This type of interactions produces emulsions with higher stable volume fraction and with smaller emulsion droplets.[39] In the case of h-BNNS, the interactions between the h-BN p-orbitals and π-orbitals of the solvent are weaker, and therefore the emulsion droplets become larger.

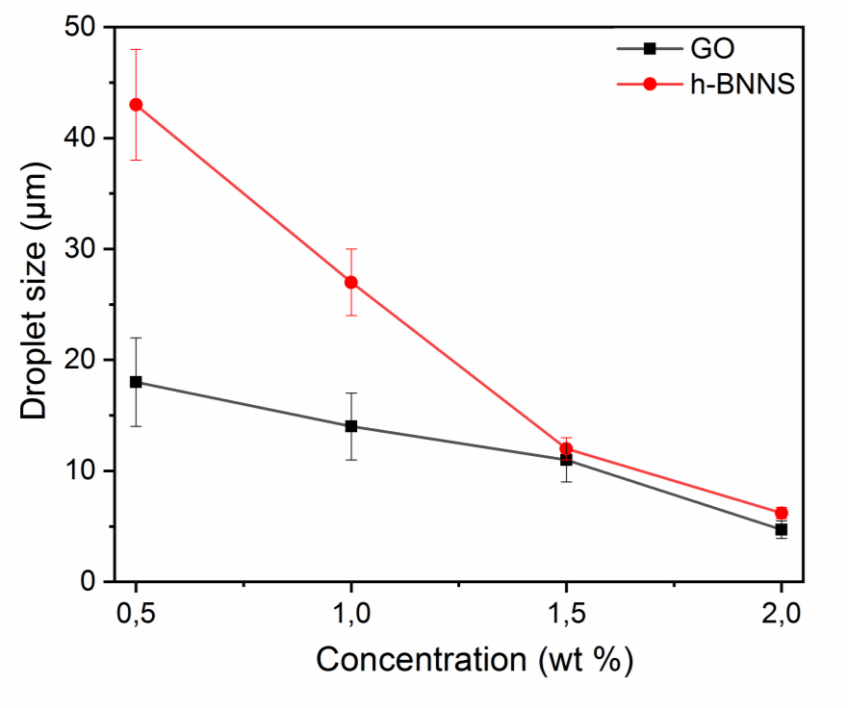

Figure 11 Mean droplet size of GO and h-BNNS stabilized emulsions at different concentrations

3.7 Emulsions stability

The GO and h-BNNS based-emulsions were stored at room temperature for 14 days and their stability was followed by eyes. The results of the stability of GO and h-BNNS based emulsions at different concentrations and various O/W ratios are presented in **Table S1** and **Table S2**, respectively**.** Either in the emulsions stabilized by GO or in those stabilized with h-BNNS, the most stable emulsions are those formulated with higher nanosheets concentration (2 wt%). The emulsions stability index (ESI) goes up to 94 % in the case of h-BNNS based emulsions and 96 % for GO based emulsions when the emulsion is formulated with 2 wt% and o/w ratio of 1. The ESI, for both GO and h-BNNS emulsions, decreases with the decrease of concentration as well as with the decrease of Φ_{dp}. It was observed that the emulsion destabilizes in two phases, one is the emulsified fraction and the other phase is resulting from

the separation of the continuous phase. **Figure 12** presents a photographic image of emulsions stabilized by h-BNNS and GO taken after 14 days. It can be observed two different behaviors related to emulsion destabilization. In the case of GO emulsions, a phase can be distinguished at the top of the emulsion resulting from the creaming of the water phase (mass density at 20°C is 1000 kg m^{-1}) when is separated from the emulsion fraction. Conversely for h-BNNS stabilized emulsions, we observed a phase at the bottom of the emulsion: the oil that tends to sediment due to its higher density (mass density at 20°C is 1045 kg m^{-1}).

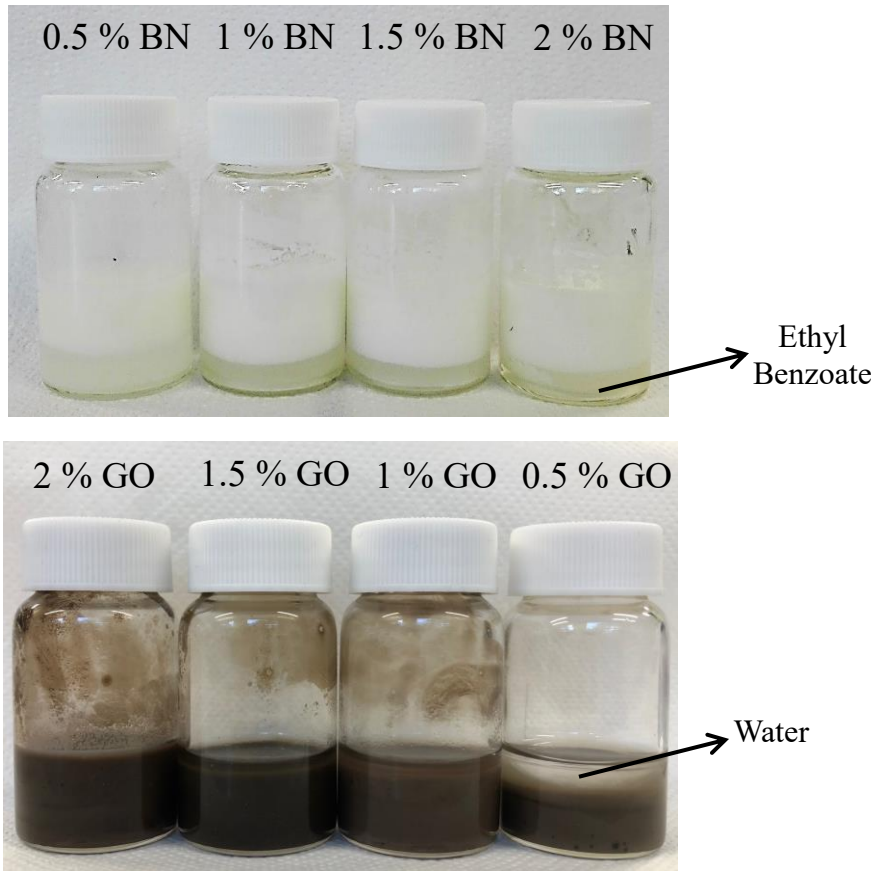

Figure 12 Photographs of the appearance of emulsions stabilized by different concentrations of h-BNNS (top image) and GO (bottom image) with o/w ratio 1 after 14 days emulsification.

Figure 13 shows the evolution of the emulsified fraction with time of GO (bottom graphic) and h-BNNS (top graphic) emulsions formulated at 2 wt% and different O/W ratios. In both type of emulsions, O/W and W/O, the destabilization of emulsions formulated at lower concentration occurs faster than for those formulated with higher concentration. This fact is due to the particle concentration effect, which is an important factor in the formation of Pickering emulsions. The increase of particle concentration induces the migration of the particles from the dispersion media, aqueous dispersion for GO and oil phase for h-BNNS, onto the oil-water interface.

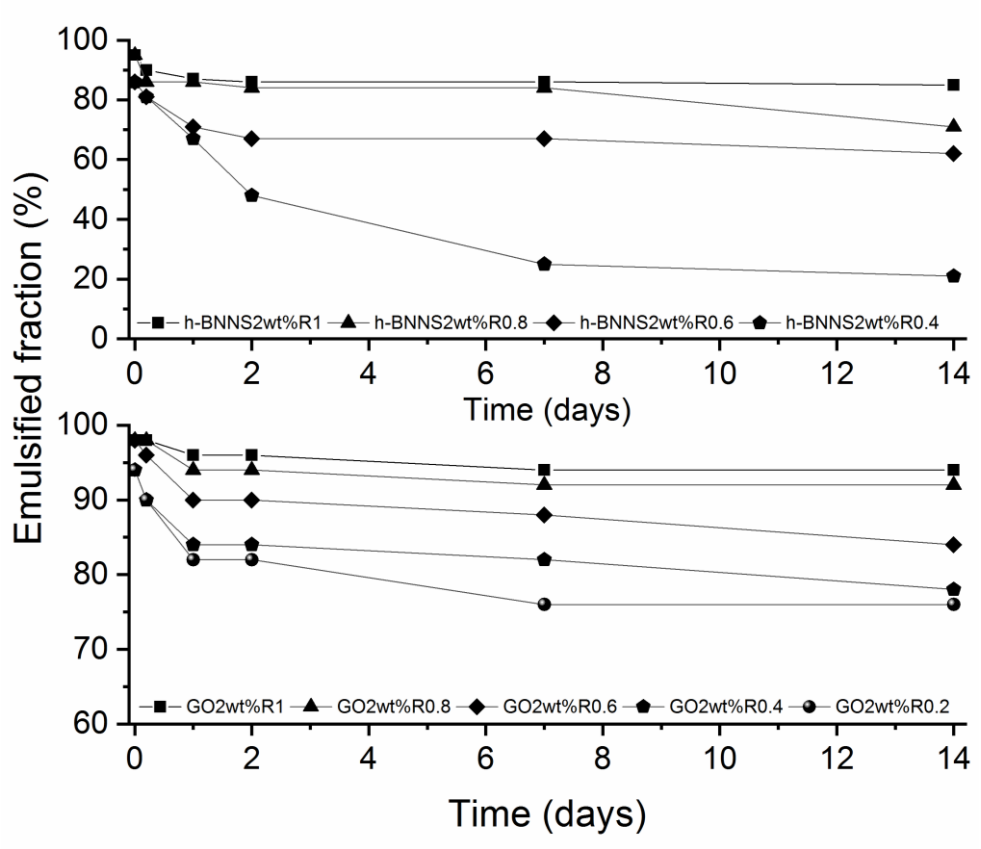

Figure 13 Emulsified fraction of a) O/W emulsions prepared with 2 wt% GO and b) W/O emulsions prepared with 2wt% h-BNNS at different o/w ratios

This phenomenon reduces the surface energy of the system by increasing the particles surface area and causing a direct reduction in the free energy, making the system more stable.[58], [59] Thus, we can conclude that the formation of Pickering emulsion with greater stability could be facilitated by increasing the particle concentration within a certain range, resulting in an increase of the total surface area of particles assembling at liquid-liquid interfaces.

3.8 Rheological studies

The effect of water volume fraction on the rheological properties of the GO and h-BNNS stabilized emulsions was studied by diluting the emulsion at constant particle concentration (2wt %) and thus keeping the droplets size distribution unchanged. **Figure 14** shows the viscosity and flow curves of GO and h-BNNS. The results shown are for measurement made while increasing shear rate, but similar trends are obtained as the shear rate decreases. At low shear rates, the emulsion shear stress remains approximately constant; at higher shear rates, the stress increases as a roughly linear function of the shear rate. This change in flow behavior suggests that the emulsions have a small yield stress at rest, which increases with increasing the volume fraction.

The existence of yield stress indicates the presence of interactions between droplets. In terms of emulsions viscosity, both GO and h-BNNS emulsion, display a shear thinning flow behavior, characterized by decreasing the viscosity as shear rate increases. This phenomenon could be attributed to droplets organization. At rest, the droplets present a higher close packing; when a shear rate is applied, the droplets start to be organized into layers or strings leading to viscosity decrease. The viscosity of GO and h-BNNS was measured at two different shear rates, 50 and 100 s^{-1}. The values are shown in **Table 2** and **Table 3** for GO and h-BNNS stabilized emulsions, respectively. In the case of GO stabilized emulsion, the higher

viscosity was found to be 282 ± 11 mPa·s and 149 ± 9 mPa·s, at 50 and 100 s^{-1} respectively, for an O/W ratio of 0.8 which corresponds to Φ_o = 0.44. For h-BNNS stabilized emulsions formulated with an O/W ratio of 0.7 which corresponds to Φ_w = 0.59, it was found a lower viscosity of 132 ± 12 mPa·s and 78 ± 1 mPa·s, for 50 and 100 s^{-1} respectively.

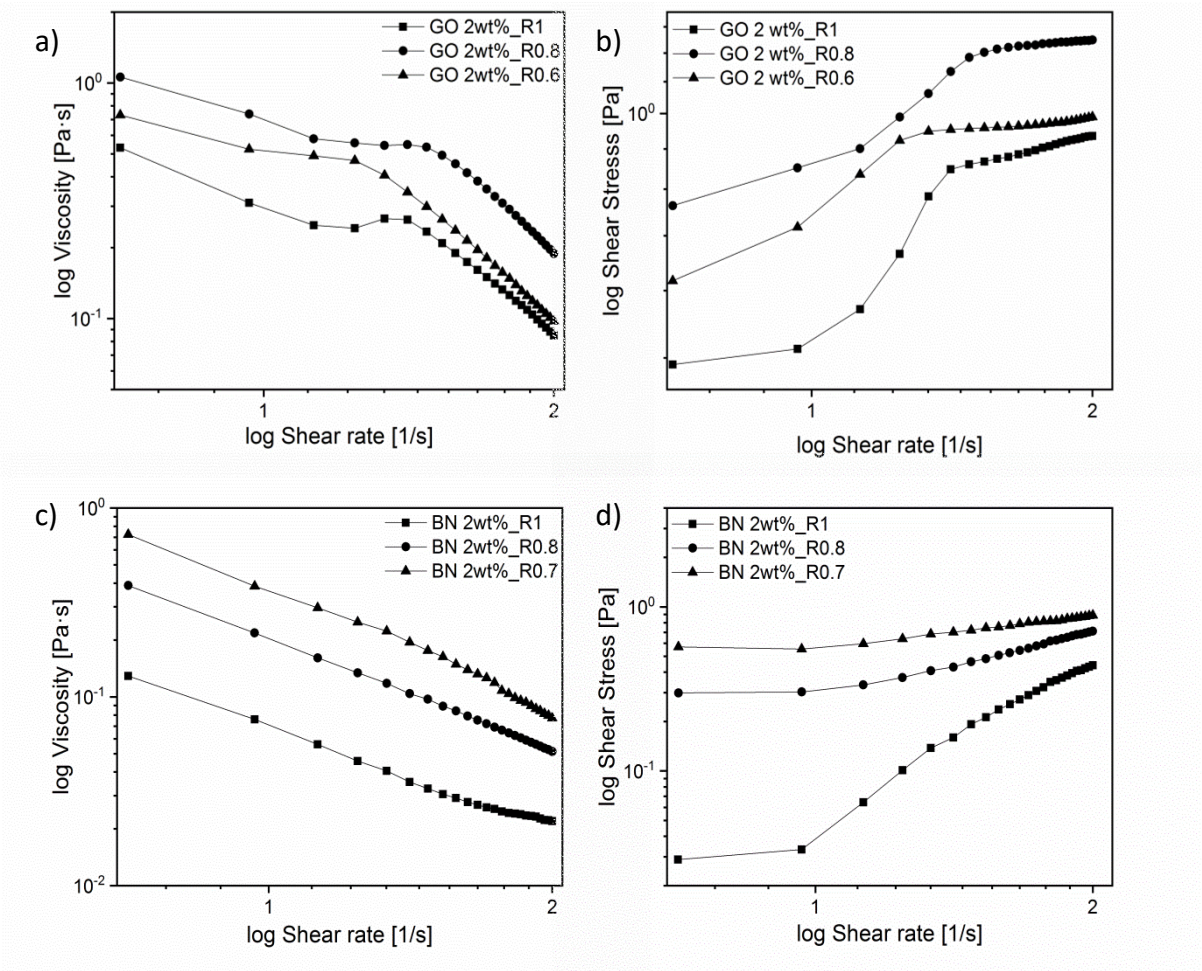

Figure 14 a) Viscosity and b) flow curves of O/W emulsions with 2 wt% GO and different o/w ratios (R=0.6 to 1); c Viscosity and d) flow curves of W/O emulsions with 2 wt% h-BNNS and different o/w ratios (R=0.7 to 1)

The GO emulsions viscosity is higher for all the O/W ratios than the viscosity of h-BNNS based emulsions, even if the dispersed phase volume fraction is higher for h-BNNS (Φ_w = 0.59) compared to those of GO (Φ_o = 0.44). This fact could be explained due to the π-π interactions between the partially broken sp^2 carbon networks of GO and the benzene rings present in the ethyl benzoate, as it was mentioned before. These interactions produce emulsions with higher stable volume fraction and therefore higher viscosity.

Table 2 Viscosity values of emulsion with 2 wt% GO for 0.6, 0.8 and 1 o/w ratio.

	GO 2 wt% R0.6	**GO 2 wt % R0.8**	**GO 2 wt% R1**
Viscosity (mPa·s) at 50s^{-1}	181 ± 7^{a}	282 ± 11^{b}	154 ± 15^{c}
Viscosity (mPa·s) at 100s^{-1}	98 ± 7^{A}	149 ± 9^{B}	88 ± 3^{C}

Table 3 Viscosity values of emulsion with 2 wt% BN for 0.7, 0.8 and 1 o/w ratio.

	BN 2 wt% R0.7	**BN 2 wt % R0.8**	**BN 2 wt% R1**
Viscosity (mPa·s) at 50s^{-1}	132 ± 12^{a}	76 ± 7^{b}	27 ± 7^{c}
Viscosity (mPa·s) at 100s^{-1}	78 ± 1^{A}	52 ± 1^{B}	22 ± 6^{C}

4 Conclusion

In conclusion, two different types of emulsions, either oil-in-water or water-in-oil, can be produced using two-dimensional materials, i.e. GO and h-BNNS, as stabilizers. The emulsions tend to show good stability at high and intermediate oil/water ratios. Microscopy images showed that the emulsions have a relatively homogeneous droplet size distribution, and the average droplet size can be tuned with particles concentration. Emulsion droplets are smaller at higher particle concentration, at 2 wt% GO and h-BNNS the average particle sizes was found to be 4.7 and 6.2 μm, respectively. The rheological behaviors of both O/W and W/O emulsions were investigated. All the emulsions exhibit yield stress indicating interactions between droplets. GO based-emulsions display smaller droplets size and higher viscosity than h-BNNS based-emulsions. These facts are explained by the stronger π-π interactions between partially broken sp^2 carbon network on GO and the aromatic ring in the ethyl benzoate, than the π-π interactions between the sp^2 network in h-BNNS with benzene rings of ethyl benzoate. This research paves the way for the fabrication of graphene or h-BNNS based functional materials with novel nanostructures and microstructures using Pickering emulsions as soft-templates. Depending on the potential application, it is possible to tune the emulsion type, W/O or O/W, by choosing the 2D material presenting interesting properties for the applications.

References

1. Novoselov, K.S.; Geim, A.K.; Morozov, S.V.; Jiang, D.; Zhang, Y.; Dubonos, S.V.; Grigorieva, I.V.; Firsov, A.A. Electric field effect in atomically thin carbon films. *Science* **2004**, *306*, 666-669.
2. Huang, X.; Qi, X.; Boey, F.; Zhang, H. Graphene-based composites. *Chemical Society Reviews* **2012**, *41*, 666-686.
3. Huang, X.; Yin, Z.; Wu, S.; Qi, X.; He, Q.; Zhang, Q.; Yan, Q.; Boey, F.; Zhang, H. Graphene-based materials: Synthesis, characterization, properties, and applications. *Small* **2011**, *7*, 1876-1902.
4. Mak, K.F.; Lee, C.; Hone, J.; Shan, J.; Heinz, T.F. Atomically thin mos 2: A new direct-gap semiconductor. *Physical review letters* **2010**, *105*, 136805.
5. Nicolosi, V.; Chhowalla, M.; Kanatzidis, M.G.; Strano, M.S.; Coleman, J.N. Liquid exfoliation of layered materials. *Science* **2013**, *340*, 1226419.
6. Xu, M.; Liang, T.; Shi, M.; Chen, H. Graphene-like two-dimensional materials. *Chemical reviews* **2013**, *113*, 3766-3798.
7. Stoller, M.D.; Park, S.; Zhu, Y.; An, J.; Ruoff, R.S. Graphene-based ultracapacitors. *Nano letters* **2008**, *8*, 3498-3502.
8. Novoselov, K.S.; Geim, A.K.; Morozov, S.; Jiang, D.; Katsnelson, M.; Grigorieva, I.; Dubonos, S.; Firsov; AA. Two-dimensional gas of massless dirac fermions in graphene. *nature* **2005**, *438*, 197.
9. Novoselov, K.S.; Jiang, Z.; Zhang, Y.; Morozov, S.; Stormer, H.L.; Zeitler, U.; Maan, J.; Boebinger, G.; Kim, P.; Geim, A.K. Room-temperature quantum hall effect in graphene. *Science* **2007**, *315*, 1379-1379.
10. Lee, C.; Wei, X.; Kysar, J.W.; Hone, J. Measurement of the elastic properties and intrinsic strength of monolayer graphene. *Science* **2008**, *321*, 385-388.
11. Balandin, A.A.; Ghosh, S.; Bao, W.; Calizo, I.; Teweldebrhan, D.; Miao, F.; Lau, C.N. Superior thermal conductivity of single-layer graphene. *Nano letters* **2008**, *8*, 902-907.
12. Bolotin, K.; Sikes, K.; Hone, J.; Stormer, H.; Kim, P. Temperature-dependent transport in suspended graphene. *Physical review letters* **2008**, *101*, 096802.
13. Lou, Z.; Chen, S.; Wang, L.; Jiang, K.; Shen, G. An ultra-sensitive and rapid response speed graphene pressure sensors for electronic skin and health monitoring. *Nano Energy* **2016**, *23*, 7-14.
14. Shen, T.-Z.; Hong, S.-H.; Song, J.-K. Electro-optical switching of graphene oxide liquid crystals with an extremely large kerr coefficient. *Nature materials* **2014**, *13*, 394.
15. Tao, H.; Gao, Y.; Talreja, N.; Guo, F.; Texter, J.; Yan, C.; Sun, Z. Two-dimensional nanosheets for electrocatalysis in energy generation and conversion. *Journal of Materials Chemistry A* **2017**, *5*, 7257-7284.
16. Larcher, D.; Tarascon, J.-M. Towards greener and more sustainable batteries for electrical energy storage. *Nature chemistry* **2015**, *7*, 19.
17. Yin, P.T.; Shah, S.; Chhowalla, M.; Lee, K.-B. Design, synthesis, and characterization of graphene–nanoparticle hybrid materials for bioapplications. *Chemical reviews* **2015**, *115*, 2483-2531.
18. Varghese, S.S.; Lonkar, S.; Singh, K.; Swaminathan, S.; Abdala, A. Recent advances in graphene based gas sensors. *Sensors and Actuators B: Chemical* **2015**, *218*, 160-183.
19. Pakdel, A.; Bando, Y.; Golberg, D. Nano boron nitride flatland. *Chemical Society Reviews* **2014**, *43*, 934-959.

20. Wang, X.; Zhi, C.; Weng, Q.; Bando, Y.; Golberg, D. In *Boron nitride nanosheets: Novel syntheses and applications in polymeric composites*, Journal of Physics: Conference Series, 2013; IOP Publishing: p 012003.
21. Ouyang, T.; Chen, Y.; Xie, Y.; Yang, K.; Bao, Z.; Zhong, J. Thermal transport in hexagonal boron nitride nanoribbons. *Nanotechnology* **2010**, *21*, 245701.
22. Golberg, D.; Bando, Y.; Huang, Y.; Terao, T.; Mitome, M.; Tang, C.; Zhi, C. Boron nitride nanotubes and nanosheets. *ACS nano* **2010**, *4*, 2979-2993.
23. Chen, Y.; Zou, J.; Campbell, S.J.; Le Caer, G. Boron nitride nanotubes: Pronounced resistance to oxidation. *Applied physics letters* **2004**, *84*, 2430-2432.
24. Li, L.H.; Cervenka, J.; Watanabe, K.; Taniguchi, T.; Chen, Y. Strong oxidation resistance of atomically thin boron nitride nanosheets. *ACS nano* **2014**, *8*, 1457-1462.
25. Bechelany, M.; Brioude, A.; Stadelmann, P.; Bernard, S.; Cornu, D.; Miele, P. Preparation of bn microtubes/nanotubes with a unique chemical process. *The Journal of Physical Chemistry C* **2008**, *112*, 18325-18330.
26. Bernard, S.; Salles, V.; Li, J.; Brioude, A.; Bechelany, M.; Demirci, U.B.; Miele, P. High-yield synthesis of hollow boron nitride nano-polyhedrons. *Journal of Materials Chemistry* **2011**, *21*, 8694-8699.
27. Gonzalez Ortiz, D.; Pochat-Bohatier, C.; Cambedouzou, J.; Bechelany, M.; Miele, P. Exfoliation of hexagonal boron nitride (h-bn) in liquide phase by ion intercalation. *Nanomaterials* **2018**, *8*, 716.
28. Lewinski, N.; Colvin, V.; Drezek, R. Cytotoxicity of nanoparticles. *Small* **2008**, *4*, 26-49.
29. Pinto, A.M.; Goncalves, I.C.; Magalhães, F.D. Graphene-based materials biocompatibility: A review. *Colloids and Surfaces B: Biointerfaces* **2013**, *111*, 188-202.
30. Chen, X.; Wu, P.; Rousseas, M.; Okawa, D.; Gartner, Z.; Zettl, A.; Bertozzi, C.R. Boron nitride nanotubes are noncytotoxic and can be functionalized for interaction with proteins and cells. *Journal of the American Chemical Society* **2009**, *131*, 890-891.
31. Ciofani, G.; Danti, S.; Genchi, G.G.; Mazzolai, B.; Mattoli, V. Boron nitride nanotubes: Biocompatibility and potential spill-over in nanomedicine. *Small* **2013**, *9*, 1672-1685.
32. Weng, Q.; Wang, B.; Wang, X.; Hanagata, N.; Li, X.; Liu, D.; Wang, X.; Jiang, X.; Bando, Y.; Golberg, D. Highly water-soluble, porous, and biocompatible boron nitrides for anticancer drug delivery. *ACS nano* **2014**, *8*, 6123-6130.
33. Weber, M.; Koonkaew, B.; Balme, S.; Utke, I.; Picaud, F.; Iatsunskyi, I.; Coy, E.; Miele, P.; Bechelany, M. Boron nitride nanoporous membranes with high surface charge by atomic layer deposition. *ACS applied materials & interfaces* **2017**, *9*, 16669-16678.
34. Nasr, M.; Viter, R.; Eid, C.; Habchi, R.; Miele, P.; Bechelany, M. Enhanced photocatalytic performance of novel electrospun bn/tio 2 composite nanofibers. *New Journal of Chemistry* **2017**, *41*, 81-89.
35. Biscarat, J.; Bechelany, M.; Pochat-Bohatier, C.; Miele, P. Graphene-like bn/gelatin nanobiocomposites for gas barrier applications. *Nanoscale* **2015**, *7*, 613-618.
36. Nagarajan, S.; Belaid, H.; Pochat-Bohatier, C.; Teyssier, C.; Iatsunskyi, I.; Coy, E.; Balme, S.; Cornu, D.; Miele, P.; Kalkura, N.S. Design of boron nitride/gelatin electrospun nanofibers for bone tissue engineering. *ACS applied materials & interfaces* **2017**, *9*, 33695-33706.
37. Eda, G.; Chhowalla, M. Chemically derived graphene oxide: Towards large-area thin-film electronics and optoelectronics. *Advanced Materials* **2010**, *22*, 2392-2415.

38. Kim, J.; Cote, L.J.; Kim, F.; Yuan, W.; Shull, K.R.; Huang, J. Graphene oxide sheets at interfaces. *Journal of the American Chemical Society* **2010**, *132*, 8180-8186.
39. He, Y.; Wu, F.; Sun, X.; Li, R.; Guo, Y.; Li, C.; Zhang, L.; Xing, F.; Wang, W.; Gao, J. Factors that affect pickering emulsions stabilized by graphene oxide. *ACS applied materials & interfaces* **2013**, *5*, 4843-4855.
40. Imperiali, L.; Clasen, C.; Fransaer, J.; Macosko, C.W.; Vermant, J. A simple route towards graphene oxide frameworks. *Materials Horizons* **2014**, *1*, 139-145.
41. Thickett, S.C.; Zetterlund, P.B. Graphene oxide (go) nanosheets as oil-in-water emulsion stabilizers: Influence of oil phase polarity. *Journal of colloid and interface science* **2015**, *442*, 67-74.
42. Creighton, M.A.; Ohata, Y.; Miyawaki, J.; Bose, A.; Hurt, R.H. Two-dimensional materials as emulsion stabilizers: Interfacial thermodynamics and molecular barrier properties. *Langmuir* **2014**, *30*, 3687-3696.
43. Gonzalez Ortiz, D.; Pochat-Bohatier, C.; Cambedouzou, J.; Balme, S.; Bechelany, M.; Miele, P. Inverse pickering emulsion stabilized by exfoliated hexagonal-boron nitride (h-bn). *Langmuir* **2017**, *33*, 13394-13400.
44. Han, Y.; Ge, Y.; Chao, Y.; Wang, C.; Wallace, G.G. Recent progress in 2d materials for flexible supercapacitors. *Journal of energy chemistry* **2017**.
45. Fowkes, F.M. Calculation of work of adhesion by pair potential suummation. *Journal of colloid and interface science* **1968**, *28*, 493-505.
46. Owens, D.K.; Wendt, R. Estimation of the surface free energy of polymers. *Journal of Applied Polymer Science* **1969**, *13*, 1741-1747.
47. Annamalai, M.; Gopinadhan, K.; Han, S.A.; Saha, S.; Park, H.J.; Cho, E.B.; Kumar, B.; Kim, S.-W.; Venkatesan, T. On the nature of wettability of van der waals heterostructures. *Nanoscale* **2016**, *8*, 5764-5770.
48. Wan, W.; Zhao, Z.; Hughes, T.C.; Qian, B.; Peng, S.; Hao, X.; Qiu, J. Graphene oxide liquid crystal pickering emulsions and their assemblies. *Carbon* **2015**, *85*, 16-23.
49. Min, T.H.; Lee, C.J.; Choi, H.J. Pickering emulsion polymerized core-shell structured poly (methyl methacrylate)/graphene oxide particles and their electrorheological characteristics. *Polymer Testing* **2018**.
50. Suresh, I.; Chidambaram, K.; Vinod, V.; Rajender, N.; Venkateswara, R.M.; Miroslav, Č. Synthesis, characterization and optical properties of graphene oxide–polystyrene nanocomposites. *Polymers for Advanced Technologies* **2015**, *26*, 214-222.
51. Luo, J.; Cote, L.J.; Tung, V.C.; Tan, A.T.; Goins, P.E.; Wu, J.; Huang, J. Graphene oxide nanocolloids. *Journal of the American Chemical Society* **2010**, *132*, 17667-17669.
52. Pakdel, A.; Zhi, C.; Bando, Y.; Nakayama, T.; Golberg, D. Boron nitride nanosheet coatings with controllable water repellency. *ACS nano* **2011**, *5*, 6507-6515.
53. Gonzalez-Ortiz, D.; Pochat-Bohatier, C.; Gassara, S.; Cambedouzou, J.; Bechelany, M.; Miele, P. Development of novel h-bnns/pva porous membranes via pickering emulsion templating. *Green Chemistry* **2018**, *20*, 4319-4329.
54. Marcano, D.C.; Kosynkin, D.V.; Berlin, J.M.; Sinitskii, A.; Sun, Z.; Slesarev, A.; Alemany, L.B.; Lu, W.; Tour, J.M. Improved synthesis of graphene oxide. *ACS nano* **2010**, *4*, 4806-4814.
55. Gao, W. The chemistry of graphene oxide. In *Graphene oxide*, Springer: 2015; pp 61-95.
56. Li, H.; Zeng, X.C. Wetting and interfacial properties of water nanodroplets in contact with graphene and monolayer boron–nitride sheets. *ACS nano* **2012**, *6*, 2401-2409.
57. Li, X.; Qiu, H.; Liu, X.; Yin, J.; Guo, W. Wettability of supported monolayer hexagonal boron nitride in air. *Advanced Functional Materials* **2017**, *27*, 1603181.

58. Aveyard, R.; Binks, B.P.; Clint, J.H. Emulsions stabilised solely by colloidal particles. *Advances in Colloid and Interface Science* **2003**, *100*, 503-546.
59. Gudarzi, M.M.; Sharif, F. Self assembly of graphene oxide at the liquid–liquid interface: A new route to the fabrication of graphene based composites. *Soft Matter* **2011**, *7*, 3432-3440.